J Mol Model (2017) 23: 244
DOI 10.1007/s00894-017-3421-x

ORIGINAL PAPER

Modification of 56A$_{CARBO}$ force field for molecular dynamic calculations of chitosan and its derivatives

Vladimir S. Naumov[1,2] · **Stanislav K. Ignatov**[1]

Received: 24 October 2016 / Accepted: 14 July 2017 / Published online: 26 July 2017

Abstract The GROMOS 56A$_{CARBO}$ force field for the description of carbohydrates was modified for calculations of chitosan (poly–1,4–(N–acetyl)–β–D–glucopyranosamine–2) with protonated and non-protonated amino groups and its derivatives. Additional parameterization was developed on the basis of quantum chemical calculations. The modified force field (56A$_{CARBO_CHT}$) allows performing the molecular dynamic calculations of chitosans with different degrees of protonation corresponding to various acidity of medium. Test calculations of the conformational transitions in the chitosan rings and polymeric chains as well as the chitosan nanocrystal dissolution demonstrate good agreement with experimental data.

Keywords Chitosan · Chitin · Molecular dynamics · 56A$_{CARBO}$ · Force field extension

Introduction

The derivatives of amino-substituted polyglycans, in particular, chitosan (poly–1,4–(N–acetyl)–β–D–glucopyranosamine–2), are nowadays considered as perspective means for the drug encapsulation and drug transport in an organism [1–3]. They are convenient, non-toxic, and easily derivable agents interacting with biological structures (cell membranes, walls, receptors, etc.) which is especially important for the development of modern medicinal systems with active targeting [4]. However, practical application of these compounds is complicated by the lack of data on the structure of their chains or globules in aqueous solutions and also on thermodynamic properties and kinetics of the complex formation in aquatic environment. In particular, the interpretation of polymer chain structure in the solution based on electron microscopy data [5–7] raised a discussion. The data on instability constants upon interaction with different protein agents are almost absent, and the dissolution process itself and its kinetics have been mainly studied using experimental methods based on the formal kinetic approach. Chitosan is a mixture of polymers with various degrees of acetylation, molecular weight and arrangement of acetyl groups in the polymer chain and its aqueous solutions are characterized by additional protonation of free amino groups. Therefore, experimental study may often provide only apparent or averaged physicochemical characteristics. In this respect, the molecular dynamic method applied for investigation of chitosan dissolution and complex formation processes is one of the approaches ensuring determination of actual thermodynamic and kinetic constants. Besides, the molecular dynamic investigation ensures much more detailed study of regularities associated with changes in these constants upon variation of number, charge, and type of chitosan chain substitutes, their length, peculiarities of their interaction between each other and with other molecules, surfaces or particles of the considered system.

In many cases, the molecular dynamic studies are performed using the simplified coarse-graining models [8] and/or the implicit solvent models which enable simulation of large-size systems. Examples of such studies are described in the refs [9–11]. However, such a simulation often requires verification

Electronic supplementary material The online version of this article (doi:10.1007/s00894-017-3421-x) contains supplementary material, which is available to authorized users.

✉ Vladimir S. Naumov
vsnaumov@yandex.ru

[1] N.I. Lobachevsky State University of Nizhny Novgorod, 23 Gagarin Avenue, Nizhny Novgorod, Russia 603950

[2] Research institute of chemistry of University of Nizhny Novgorod, 23 Gagarin Avenue, Nizhny Novgorod, Russia 603950

including those based on atomistic models where interactions between polymer and solvent atoms are evidently considered by inclusion of corresponding intra- and intermolecular potentials into the force field. In the case of atomistic molecular dynamic simulations of polyglucan derivatives, one of the most up-to-date and prospective force fields is the $56A_{CARBO}$ [12] force field which is a part of the GROMOS [12–17] force field family. It has been specially adapted for the description of polymer chains based on monomer units of hexapyranose and is an extension of the force field 53A6 [13], which is aimed at simulations of biomolecules. Some examples of the chitosan studies using the GROMOS force fields are described in refs [18, 19]. Recently, a new $56A_{CARBO}$-based force field revision $56A_{CARBO\_R}$ was proposed [17] on the basis of thorough analysis of ring-conformational equilibria [20, 21]. This force field significantly improves the description of conformational features of hexopyranose and its derivatives. Nevertheless, $56A_{CARBO}$ force field and its known extensions do not include monomer residues of aminopyranose which makes it impossible to use it for calculations of chitosan and its derivatives. As an alternative to $56A_{CARBO}$, there are universal force fields and automated force field builders which can be applied to a wide range of molecules [22]. However, although these approaches are useful in terms of universalization, the manual force field parameter adjustment with careful correspondence to the original reliable parametrization scheme, i.e., $56A_{CARBO}$ in our case, gives more accurate results. In this work we extend the force field for the molecular dynamic simulations of chitosan and its derivatives by adding the new parameters for the residues of aminopyranose, acetyl aminopyranose, and protonated form of aminopyranose to the $56A_{CARBO}$ parameter set. The special emphasis of this force field extension is the description of dissolution and association processes of chitosan and its derivatives for the modeling of absorption and encapsulation of various organic and inorganic agents.

Force field modification

GROMOS $56A_{CARBO}$ force field refers to the group of force fields with united atoms making allowance for solvent molecules in an explicit form and includes both intermolecular and intramolecular potentials. Within this force field it is suggested that biopolymer molecules are subdivided into monomer fragments which are referred to as residues by analogy with protein molecules. Various molecular structures may be obtained by connecting residues in different ways.

The intermolecular interactions between atoms of different residues are determined by Coulomb interactions and van der Waals forces. Atomic charges in a residue are determined on the basis of the bond–increment approach [23, 24] when neighboring atoms influence the charge of the central atom. This approach is used only for oxygen-containing bonds. "Charge groups" include the atoms surrounding the oxygen atom and chemically bonded to it. The charge group should be generally neutral, the only exception is made for some systems (polyesters) which may contain charged groups to avoid formation of very large groups. The rules for determination of charge groups are illustrated in Fig. 1 which shows the glucose molecule with charge groups arranged according to $56A_{CARBO}$ rules.

The $56A_{CARBO}$ force field contains the residues of β–D–glucopyranose (GLC, GLCN, GLC0). The force field parameters for these residues have been chosen according to results of glucose quantum chemical calculation in vacuum performed at the B3LYP/6–311+G(d,p) level [12]. The main structural element of chitosan is β–D–glucopyranosamine–2 (very similar to β–D–glucopyranose). To describe chitosan within the $56A_{CARBO}$ field substitution of the C2 hydroxyl group in GLC-residues by a free, protonated or substituted (for instance, acetylated) amino group is required. Thus, the force field should be supplemented with residues CHT0, CHTN, CHT, CHTP, CHTR (Fig. 2).

The modification of the residues structure suggests (1) change of charges in glucopyranose ring atoms; (2) determination of a new charge group; (3) selection of new parameters for bonds, valence angles, and dihedral angles for atom groups which are absent in glucopyranose residues.

The charge distribution in the charge group C2 (Fig. 1) is determined using the above mentioned bond–increment approach. If the OH group at the C2 atoms is substituted by NH_2, the parameters of the charge displacement from additional hydrogen to nitrogen ($\Delta q_{H\rightarrow N}$) and from carbon to nitrogen ($\Delta q_{C\rightarrow N}$) can be determined. In this work, the atomic charges within the charge groups have been determined on the basis of quantum chemical calculations. The criterion for the quantum-chemical method selection may be the proportionality of the calculated glucose atom charges relative to the

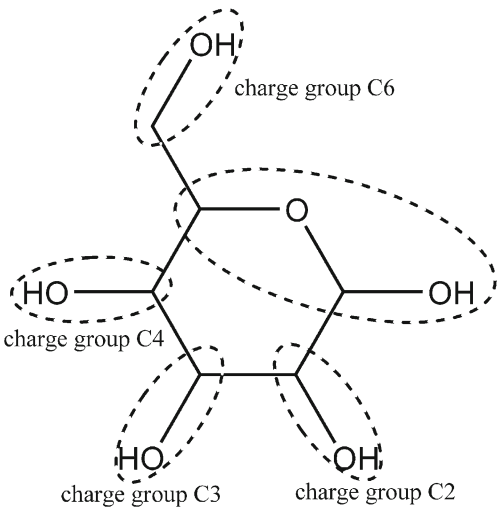

Fig. 1 Charge groups in glucose molecule selected according to $56A_{CARBO}$ force field rules

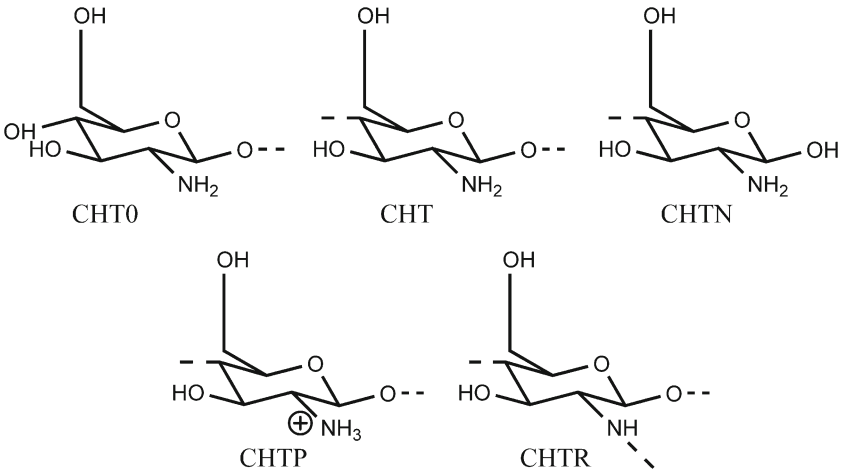

Fig. 2 Residues to be added to $56A_{CARBO}$ force field for simulation of chitosan and its amino-substituted analogs

charges in the $56A_{CARBO}$ and the neutrality of the charge groups corresponding to the original force field.

In order to find the most suitable charge calculation scheme we tried several approaches: Mulliken charges calculated at broad variations of theory levels including Hartree-Fock, DFT (BLYP, B3LYP, PBE0, M06 functionals), and the ESP-derived charges calculated using the Merz-Kollman (MK) [25] and CHelpG [26] methods. The most representative results are presented in Table 1. The full set of the calculation results concerning the atomic charges is given in Supplementary information (Table 1).

As seen from Table 1, when charges are calculated at the HF/STO–3G level, the determination coefficient (R) and its square (R^2) are very close to one which indicates a high degree of proportionality between the calculated charges and the charges in $56A_{CARBO}$ force field. The proportionality coefficient in this case is equal to 2.013, and the total charge of the considered atomic group is almost equal to zero which also confirms correlation between the HF/STO–3G charges and parameters of the force field. Thus, the Mulliken charges calculated at the HF/STO–3G level are best suited for supplementation of the force field. It seems a little unexpected that

Table 1 The atomic charges of β–D–glucopyranose calculated using various theory levels in comparison with the original $56A_{CARBO}$ values

Theory	AO basis set	qC[a]	qO [a]	qH[a]	Q_{sum}[b]	*Coef*[c]	R^{2}[c]
$56A_{CARBO}$		0.232	−0.642	0.410	0.000		
b3lyp	STO–3G	0.088	−0.298	0.206	−0.003	2.260	0.9956
	6–31G(d.p)	0.246	−0.571	0.321	−0.004	1.115	0.9932
	cc–pVTZ	0.159	−0.367	0.212	0.003	1.714	0.9943
blyp	STO–3G	0.079	−0.286	0.202	−0.005	2.404	0.9926
	6–31G(d,p)	0.230	−0.534	0.303	−0.002	1.188	0.9937
	cc–pVTZ	0.148	−0.345	0.199	0.003	1.830	0.9945
hf	STO–3G	0.116	−0.319	0.203	−0.001	2.013	1.0000
	6–31G(d,p)	0.313	−0.688	0.363	−0.011	0.935	0.9865
	cc–pVTZ	0.206	−0.443	0.242	0.005	1.423	0.9876
m06	STO–3G	0.094	−0.324	0.226	−0.004	2.088	0.9947
	6–31G(d,p)	0.253	−0.602	0.346	−0.002	1.056	0.9951
	cc–pVTZ	0.173	−0.361	0.198	0.010	1.730	0.9861
pbe0	STO–3G	0.086	−0.298	0.210	−0.003	2.268	0.9940
	6–31G(d,p)	0.235	−0.58	0.336	−0.008	1.105	0.9967
	cc–pVTZ	0.142	−0.358	0.216	0	1.775	0.9983
MK/B3PW91	6–31++G(d,p)	0.202	−0.694	0.461	−0.031	0.988	0.9968
CHelpG/B3PW91	6–31++G(d,p)	0.228	−0.701	0.454	−0.019	0.945	0.9993

[a] The atom designation corresponds to charge group C2, see Fig. 1. [b] Q_{sum} is a total charge for the correponding charge group C2 (should be zero within $56A_{CARBO}$). [c] *Coef* is the proportional coefficient between charges calculated with QM and charges defined within $56A_{CARBO}$. [d] R^2 is the determination coefficient for the correlation between the calculated charges and the charges defined within $56A_{CARBO}$

this modest level of theory provides better consistence with the original force field parameters in comparison with modern functionals and the multiple-split bases augmented by d- and *f*-polarization functions. Probably, the reason of this fact is the strong charge localization in the case of HF/STO–3G which is important for the point charge derivation. It should also be noted that the original force field charges were derived from the B3LYP/6-311G+(d,p) calculations with additional manual adjustment. It is interesting that the ESP-derived charges based on the MK and CHelpG schemes provides rather good but not ideal coincidence both with $56A_{CARBO}$ and higher level DFT charges. They also require additional scaling and the proportionality is not dramatically better than in the case of simpler Mulliken scheme. Moreover, the charge groups obtained on the basis of ESP-derived charges are not neutral. Thus, the application of these schemes, in contrast with HF/STO-3G charges, require additional manual corrections.

Table 2 lists the charges of β–D–glucopyranose obtained with the quantum-chemical calculations (HF/STO–3G) in agreement with the atom unification scheme of $56A_{CARBO}$ in comparison with the original charges of $56A_{CARBO}$. As seen from Table 2, the charges elaborated in the present work are quite close to the unified atom charges of the original force field. Thus, these results demonstrate usability of the charge determination method based on the quantum chemical calculations. In the following, we used this method for the determination of the atomic charges of the β–D–glucopyranosamine–2 along with its N-substituted and N-protonated analogs.

The β–D–glucopyranosamine–2 geometry was optimized at the B3PW91/6–31++G(d,p) level (the same, that was used for β–D–glucopyranose). Quantum-chemical calculation was performed for the condition of isolated molecule in vacuum which agrees with the method proposed by authors of $56A_{CARBO}$ force field. The calculated charges of hydrogen atoms in the amine group differ by the value (0.158 and 0.174 *e*). However, in the initial force field these atoms are equivalent, therefore their charges were averaged in the new version of the force field. Charge of C2 atom was calculated as a sum of Mulliken charges of carbon atom and covalently bound hydrogen atom. Using this method ensures that the charge group C2 has small positive charge (+0.02). In order to neutralize this charge, modules of positive charges were evenly decreased and modules of negative charges were evenly increased. The absolute value of each charge was changed by about 0.02.

The calculated Mulliken charges of the charge group C2 and the final charges obtained upon application of the above-mentioned methods are shown in Table 3 (see also Fig. 3).

Table 2 The charges of β–D–glucopyranose elaborated on the basis of quantum-chemical calculations (geometry B3PW91/6–31++G(d,p), charges HF/STO-3G), and unified in agreement with the $56A_{CARBO}$ force field

Charge group	Atom in real molecule	HF/STO–3G atom charge	Atoms of $56A_{CARBO}$[a]	Atom charge in $56A_{CARBO}$	Atom charge (this work)
C1–C5	C1	0.188	C1	0.464	0.467
	H_{C1}	0.044			
	O1	−0.319	O1	−0.642	−0.642
	H_{O1}	0.206	HO1	0.410	0.415
	O5	−0.276	O5	−0.464	−0.556
	C5	0.076	C5	0.232	0.280
	H_{C5}	0.063			
C2	C2	0.052	C2	0.232	0.234
	H_{C2}	0.064			
	O2	−0.319	O2	−0.642	−0.642
	H_{O2}	0.203	HO2	0.410	0.409
C3	C3	0.060	C3	0.232	0.229
	H_{C3}	0.054			
	O3	−0.321	O3	−0.642	−0.646
	H_{O3}	0.203	HO3	0.410	0.409
C4	C4	0.065	C4	0.232	0.242
	H_{C4}	0.055			
	O4	−0.315	O4	−0.642	−0.643
	H_{O4}	0.203	HO4	0.410	0.409
C6	C6	0.009	C6	0.232	0.266
	$H1_{C6}$	0.056			
	$H2_{C6}$	0.067			
	O6	−0.307	O6	−0.642	−0.618
	H_{O6}	0.189	HO6	0.410	0.380

[a] Some atoms in $56A_{CARBO}$ are united atoms

Table 3 Charges for atoms in C2 charge group

Atom in β–D–glucopyranosamine–2	Mulliken charge (HF/STO–3G)	Atom in CHT residue	Charge in the $56A_{CARBO\_CHT}$
Residues CHT, CHT0, CHTN (residues with free amino group)			
C2	0.027	C2	0.197
H_{C2}	0.076		
N2	−0.415	N2	−0.845
H21	0.158	H21	0.324
H22	0.174	H22	0.324
Residue CHTP (protonated amino group)			
C2	0.054	C2	0.227
H_{C2}	0.129		
N2	−0.361	N2	−0.448
H21	0.315	H21	0.407
H22	0.333	H22	0.407
H23	0.337	H23	0.407
Residue CHTR (substituted amino group)			
C2	0.044	C2	0.250
H_{C2}	0.073		
N2	−0.373	N2	−0.709
H21	0.214	H21	0.459

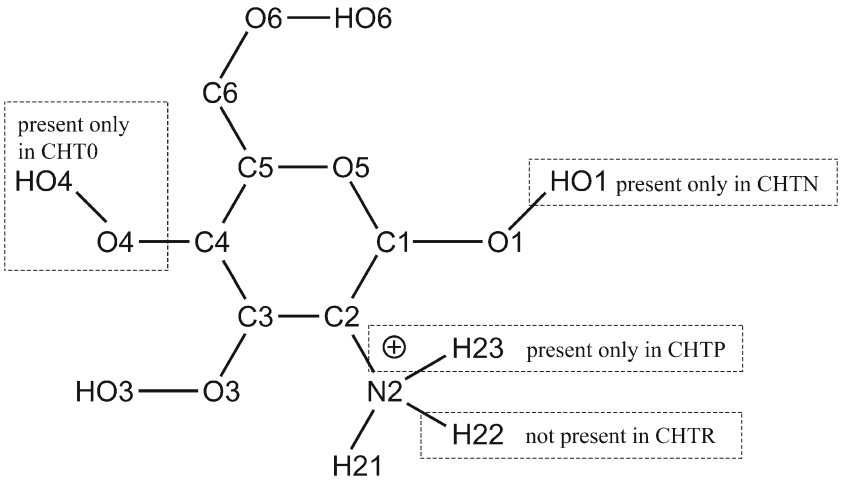

Fig. 3 N-protonated β–D–glucopyranosamine–2 with names of atoms in according to atom names in the modified force field $56A_{CARBO}$

The structure and charge parameters of the N–protonated and N–acetylated β–D–glucopyranosamine–2 were optimized at the B3PW91/6–31G(d,p) theory level because the optimization of protonated structures with diffuse functions resulted in the significant interaction between the CH_2OH and NH_2^+ groups. Due to these interactions, the CH_2OH group changed its conformation and oriented to the direction of carbohydrate ring which can potentially worsen the intramolecular potentials and lead to improper conformations in the solution. At the same time, the Mulliken charges calculated at the HF/STO-3G level for the structures optimized with or without the diffuse functions were quite close to each another (the typical deviations are within 0.002*e*).

In the case of N–protonated β–D–glucopyranosamine–2, the calculated Mulliken charge of the C2 atomic group is +0.806 whereas other group charges get additional negative increments. In order to avoid the reoptimization of all molecular group charges, it was proposed that the charge of whole molecule be condensed on C2 group, and the calculated Mulliken atomic charges within this group were scaled to provide the total group charge +1. This maintains the charges of the remaining molecular groups unchanged. Charges of the protonated C2 group which were obtained using this approach are provided in Table 3.

Two strategies may be used for selection of charge groups when extending the force field in order to describe acetylated derivatives of glucopyranosamine C2–NH–CO–CH_2X: (1) subdivision into groups C2–NH–CO and CH_2X; or (2) C2–NH and CO–CH_2X. The first method is agreed with recommendations proposed by the authors of $56A_{CARBO}$ force field. However, the second method ensures higher flexibility for further extension of the force field since it is possible to perform further simplified simulation of different N–derivatives when it is not necessary to conduct another parameterization of the charge group C2. In this case the N–substituted derivative will consist of two residues: glucopyranosamine with open nitrogen atom bonding and N–substitute (Fig. 4).

Standard constants of protonated and non-protonated NH_2 group and glucopyranose ring which are present in GROMOS 56A force field were selected as parameters of van der Waals interaction and also constants for bonds, valence angles, improper and torsional angles in residues of polyaminoglucans CHT, CHT0, CHTN, CHTP, and CHTR.

While developing $56A_{CARBO}$ force field, special attention was given to constants of dihedral angles in glucopyranose rings. When O2 was substituted by N2, some of these constants, in particular, torsional angles T3, T12, T13 (designations in accordance with [12]), were to be reparametrized.

In order to develop the above dihedral parameters we made the rigid and relaxed scan calculations for the rotations of the corresponding molecular moieties at the B3LYP/6–31++G(d,p) in vacuum and adjusted the dihedral parameters. Figure 5 demonstrates the calculated rigid scans for the rotations side group around hexopyranose ring. As seen from Fig. 5, the substitution of O-atom to N-atom does not change the shape of the potential energy curve near the energy minimum

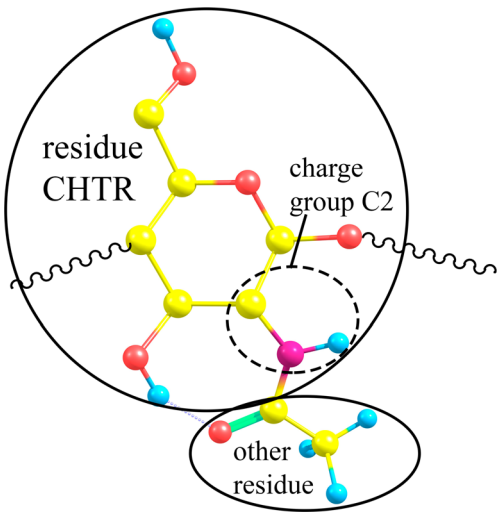

Fig. 4 Charge group selection in case of amino-substituted residue

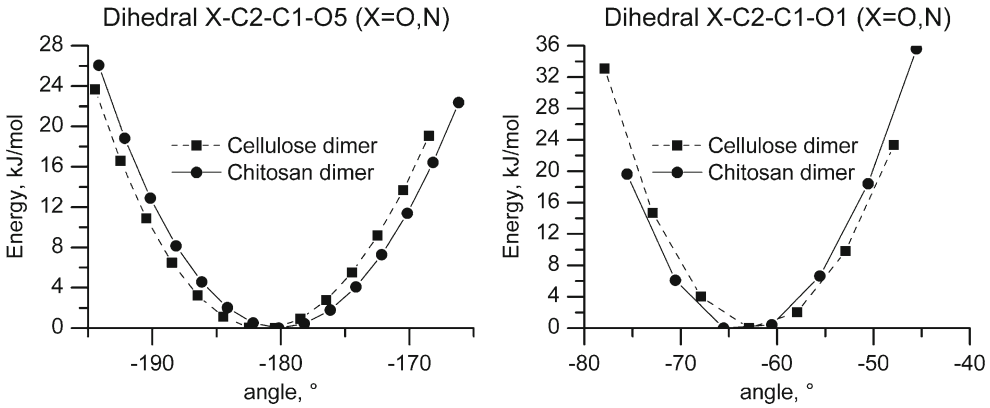

Fig. 5 Comparing energies of dihedral angles X-C2-C1-O5 and X-C2-C1-O5 (X = O,N) calculated by the rigid scan at the B3PW91/6–31++G(d,p) theory level for dimers GLC-GLC and CHT-CHT

and the PES curves for the N-substituted rings are only slightly different from the glucopyranose profiles. Thus, the $56A_{CARBO}$ parameters T12 and T13 can also be used in the case of N-substituted derivatives. This also takes place in the case of internal rotations of NH_2 group around N-C bond. Like in the original force field, the rotation of this group was adjusted using the simplified models—ethylamine and cyclohexylamine. The corresponding relaxed PES scans are shown in Fig. 6. It is interesting that the combined rotation of two hydrogen atoms around the N-C bond results in the barrier height and phase parameters very close to the parameter values for the rotation of OH group. In the case of protonated

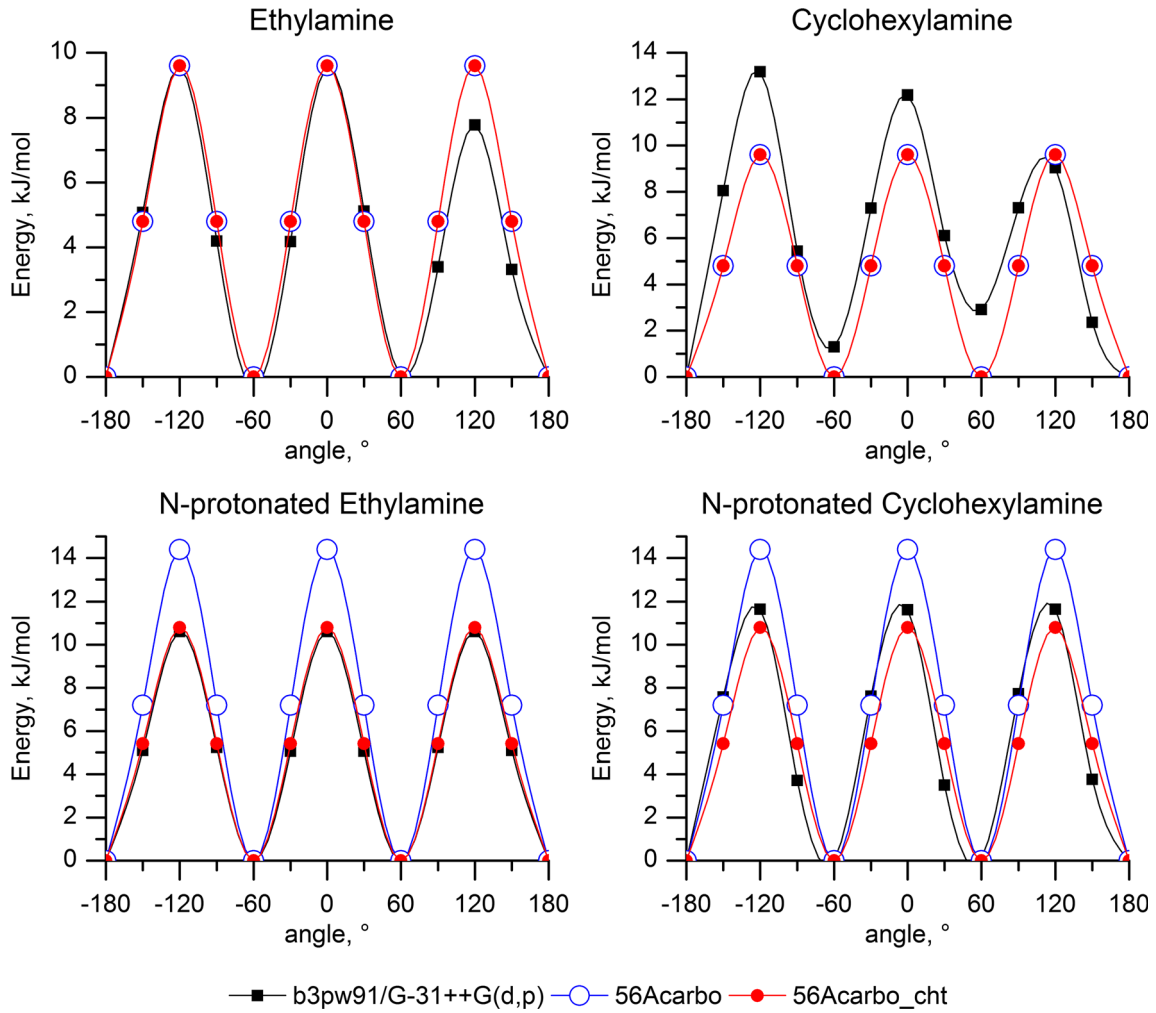

Fig. 6 Energies of rotation side group NH_2 or NH_3^+ for ethylamine and cyclohexylamine calculated by relaxed scan at the B3PW91/6–31++G(d,p) theory level, $56A_{CARBO}$, and $56A_{CARBO\_CHT}$ parametrs

amino-group NH_3^+, the barrier height parameter was decreased from 2.4 to 1.8 kJ mol^{-1} for best reproducing energy of rotation protonated amino-group, see Fig. 6 and Table 8.

In the case of Lennard-Jonnes (LJ) corrections, $56A_{CARBO}$ does not use the combination rules for the LJ parameters C_{12} as takes place in the case of C_6 parameter. Instead, it uses the GROMOS96 value with additional adjustment for this parameter to get a better agreement with the experimental data or semi-empirical schemes by Angyal [27–29] and Rao [30]. Therefore, we used the parameters for the H-O 1–5 interactions from the $56A_{CARBO}$ whereas H2N…O 1–4 parameters were taken from the corresponding NH_2 parameters of source 53A6 force field. It will be shown below that we do not observe any significant deviations from the regular chitosan conformations in an aqueous solution which can be attributed to the deficiencies of such choice.

Thus, the initial $56A_{CARBO}$ force field was supplemented with parameters of five new β–D–glucopyranosamine–2 residues for simulation of chitosan and its derivatives. The full set of these parameters is provided in Tables 4, 5, 6, 7, and 8.

The provided sets of parameters were implemented within the GROMACS program by adding data bases of force fields in a new module gromos56Acht.ff. These modules may be found in the Supplementary information attached to this article. The $56A_{CARBO}$ force field and new $56A_{CARBO\_CHT}$ force field takes into account the 1–4 and 1–5 LJ-interactions non-standard for GROMACS. To account for this interaction by standard GROMACS-subprograms, the special Python script was applied which was published earlier on the Internet by Plazinski and Drach [31]. The published tool corrects the standard GROMACS topology files and it is available for download from the official GROMACS web-site. The published script was modified according to the new CHT-residues added in the $56A_{CARBO\_CHT}$ force field. The modified script can also be found at the web site of our group [32]. It should be noted that the new modules do not contain the $56A_{CARBO\_R}$ modifications.

Simulation of structures containing residues ACE in the lateral chain leads to the problem with non-compliance of atom names within this residue which makes it impossible to develop biopolymer structures with these residues using the standard methods provided in the GROMACS program. Therefore, the force field was additionally supplemented with residue ACE2 which differs from the standard residue ACE by the name of

Table 4 Types of atoms in charge group C2 for residues with different state of amino group

Residue	C2	N2	H21	H22	H23
CHT, CHT0, CHTN	CH1R	NT	H	H	–
CHTP	CH1R	NT	H	H	H
CHTR	CH1R	N	H	–	–

Table 5 Charges of charge group C2 atoms for residues with different state of amino group

Residue	C2	N2	H21	H22	H23
CHT, CHT0, CHTN	0.197	−0.845	0.324	0.324	–
CHTP	0.227	−0.448	0.407	0.407	0.407
CHTR	0.250	−0.709	0.459	–	–

the atom adjoining the acetyl group and by presence of an additional dihedral angle $C2_{CHTR}$–$N2_{CHTR}$–C_{ACE2}–CA_{ACE2}. Standard constants of force field applied for angles of the type –C–[N, NT, NE, NZ, N]– (see item 14 of Table 5 in work [14]) were used for this angle. This structure is also included into the force field extension module for chitosans. It should be specially noted that the reparameterization of ACE2 residue was not an objective of the present work. The purpose of this study is development of parameters consistent with the current parameter sets for broad variation of substituents. Such strategy results in a non-ideal but practically useful parameterization allowing, e.g., fast screening of substituted chitosanes suitable for the purposes of encapsulating agent developments (Tables 9 and 10).

Test calculations

In order to verify the validity of the new force filed parameters, the test calculations of conformational properties of chitosan chains in the form of a nanocrystal and free polymers have been performed. The rotation barriers of exocyclic groups, the most favorable glucopyranose ring conformations, and the energy distribution of glycosidic bond conformations have been analyzed. We also carried out the simulations of the chitosan crystal dissolution in aqueous media of various acidities in order to estimate the influence of the new force field parameters on the kinetics of the chitosan dissolution.

Several sets of structural parameters differing by the packing method and presence of hydrate water in crystal lattice were published for fully deacetylated chitosan in the crystalline state [33–35]. In this work we used the crystalline structure of fully dehydrated deacetylated chitosan corresponding to data of the study [35]. The crystal model consisted of eight chitosan chains, each chain made of 20 glucopyranose units (molecular weight of the chain – 3.2 kDa). The crystal was placed at the center of the box filled with solvent molecules (SPC model of water) and chlorine counterions ensuring electrical neutrality of the solution. Dimensions of the box were 20.8 × 12.4 × 11.7 nm. The system contained about 320,000 molecules of water.

During the test MD calculations of free molecules of chitin and chitosan polymers in aqueous media, the starting geometry corresponded to the polymer chain inside the chitosan

Table 6 Parameters of bonds between atoms of charge group C2 for residues with different state of amino group

Residue	Bond	K_b (10^6•kJ•mol^{-1}•nm^{-4})	b_0 (nm)	56A$_{CARBO}$ designation	56A$_{CARBO}$ comment
CHT, CHT0, CHTN	C2–N2	8.7100	0.1470	gb_21	CHn–[N, NT, NL, NZ, NE]
	N2–H21, N2–H21	1.8700	0.1000	gb_2	H–N(all)
CHTP	C2–N2	8.7100	0.1470	gb_21	CHn–[N, NT, NL, NZ, NE]
	N2–H21, N2–H22, N2–H23	1.8700	0.1000	gb_2	H–N(all)
CHTR	C2–N2	8.7100	0.1470	gb_21	CHn–[N, NT, NL, NZ, NE]
	N2–H21	1.8700	0.1000	gb_2	H–N(all)
	N2–C$_{ACE2}$	1.0500	0.1340	gb_11	C–[N, NZ, NE]

crystal [35] with molecular mass of 4.8 kDa (30 monomeric rings). The polymer molecule was placed into the rectangular box (sizes 21.7 × 8.3 × 8.5 nm) of water with 3D periodic boundary conditions. In the chitin models, all the rings were acetylated except the terminal ones.

Molecular dynamics calculations were performed using GROMACS 4.6/5.1 software [36] with PLUMED 2.3 plugin [37] for pre-optimized NVT ensemble at 300 K (Berendsen thermostat [38] with relaxation time of 0.1 ps), Coulomb interactions were calculated with PME [39, 40], Coulomb and van-der-Waals cut-off distance was 1.5 nm (Verlet cut-off scheme). Leap-frog algorithm [41] was used for the integration step of 1 fs. Simulation time was up to 15 ns for crystalline structure and single chitosan chain. Time of simulation was increased to 19 ns for best observation of geometry parameters in the case of chitin polymers. LINCS algorithm [42] was used as a bond constraint method.

Conformational properties of exocyclic groups

Within the modified force field, the additional exocyclic group at the N2 atom (e.g., acetyl group in the chitin polymer) is characterized by torsion angle H21–N2–C2–H$_{C2}$ (χ_2), its value is related to the experimental $^3J_{HH}$ NMR constant for atoms H21 and H$_{C2}$. Additional exocyclic moieties analyzed in the test calculations were the hydroxymethyl –C6–O6–HO6 and hydroxyl –O6–HO6 groups. Rotation of the hydroxymethyl group is usually described by the angle C4–C5–C6–O6 (ω). However, another torsion angle O5–C5–C6–O6 ($\acute{\omega}$) is related to the experimental $^3J_{HH}$ value with the equations proposed by Stenutz [43] and Tafazzoli [44]. Rotation of the hydroxyl group is characterized by the angle C5–C6–O6–HO6 (χ_6). Three rotamers *g*+, *t* and *g*- correspond to three intervals of torsion angles 0–120°, 120–240°, and 240–360°, respectively.

Table 11 shows the average values of torsion angles, distributions of torsion angles in different rotamers, and the calculated $^3J_{H,H}$ values obtained in the test MD simulations of chitosan and chitin nanocrystals and polymers in comparison with the experimental and theoretical data published earlier. As evident from Table 11, the mean value of ω is in good agreement with the available XRD data, especially for the chains completely buried inside the crystal. The exocyclic groups in the surface chains are not fixed by the crystalline environment and, thus, their conformations are somewhat different from the crystalline ones. The rotamers energy

Table 7 Parameters of valence angles for residues with different state of amino group

Residue	Angle	K_θ (kJ•mol^{-1})	θ_0 (°)	56A$_{CARBO}$ designation	56A$_{CARBO}$ comment
CHT, CHT0, CHTN	C3–C2–N2, N2–C2–C1	530.00	111.00	ga_15	CHn–CHn–[C,CHn,OA,NR,NT,NL]
	C2–N2–H21, C2–N2–H22	425.00	109.50	ga_11	H–NL–[C, CHn], H–NT–CHn
	H22–N2–H21	380.00	109.50	ga_10	H–NL, NT–H, CHn–OA–CHn(sugar)
CHTP	C3–C2–N2, N2–C2–C1	530.00	111.00	ga_15	CHn–CHn–[C, CHn, OA, NR, NT, NL]
	C2–N2–H21, C2–N2–H22, C2–N2–H23	425.00	109.50	ga_11	H–NL–[C, CHn], H–NT–[CHn]
	H22–N2–H21, H23–N2–H21, H23–N2–H22	380.00	109.50	ga_10	H–[NL, NT]–H, CHn–OA–CHn(sugar)
CHTR	C3–C2–N2, N2–C2–C1	520.00	109.50	ga_13	[CHn, C]–[CHn]–[C,CHn,OA,OM,N,NE]
	C2–N2–H21	460.00	115.00	ga_18	H–N–CHn
	C2–N2–C$_{ACE2}$	700.00	122.00	ga_31	[CH1, CH2]–N–C
	H21–N2–C$_{ACE2}$	415.00	123.00	ga_32	H–N–C

Table 8 Parameters of dihedral angles for residues with different state of amino group

Residue	Angle	K_φ (kJ•mol^{-1})	$\xi_{\varphi 0}$ (°)	m_φ	56A$_{CARBO}$ designation	56A$_{CARBO}$ comment
CHT, CHT0, CHTN, CHTR	C1–C2–N2–H21, C1–C2–N2–H22	0.0	2.400	3	gdc_t3	Generic hydroxyl torsion (one per bond)
	N2–C2–C3–O3, N2–C2–C1–O1	180.0	4.500	1	gdc_t12	Oxygen–oxygen gauche torsion
	N2–C2–C1–O5	180.0	1.000	1	gdc_t13	Oxygen–oxygen intracyclic torsion
CHTP	C1–C2–N2–H21, C1–C2–N2–H22, C1–C2–N2–H23	0.0	1.800	3	no	no
Improper dihedral angles						
Residue	Angle	K_ξ (kJ•mol^{-1} •degree^{-2})	ξ_0 (degree)	–	56A$_{CARBO}$ designation	56A$_{CARBO}$ comment
CHT, CHT0, CHTN, CHTP, CHTR	C2–C3–C1–N2	0.102	35.26439	–	gi_2	tetrahedral centers

distribution and the mean value of the χ_2 angle for the molecules in a solution are also in good agreement with the previous MD simulations of Mobli and Almond [45] where the MMX [46] force field was used in a combination with NMR experimental and DFT calculated data. At the same time, these results are distinguished from the distributions of angles ω and χ_6 in the β-D-glucopyranose polymers obtained with the 56A$_{CARBO}$ and reparametrized 56A$_{CARBO_R}$ force field [17]. In our opinion, this difference reflects different properties of the unsubstituted and N-substituted pyranose rings. We conclude that the modified parameters of the amino residues represent well the properties of the N-glucosamine.

In order to represent the NMR constants, we used the equations of Stenutz et al. [43] and Tafazzoli and Ghiasi [44] in calculations of $^3J_{H,H}$, and the empirical formula of Karplus with the corresponding coefficients for β-D-glucopyranosamine [45] in $^3J_{H5,H6R}/^3J_{H5,H6S}$ calculations. Because the H_{C2} atom in the 56A force field is not present (included in united atom C2), its geometry parameters necessary for the χ_2 and $^3J_{H2,H21}$ evaluations were obtained using the DFT calculations (B3PW91/6–31G(d,p)) of its position relatively to C1, C2, C3 atoms in the β-D-glucopyranosamine tetramers and the coordinates of C1, C2, C3 atoms taken from the MD trajectory. The calculated values of the $^3J_{H,H}$ constant for the molecules in a solution coincide well with the experimental values $^3J_{H5,H6R}/^3J_{H5,H6S}$, the typical difference not more than 1 Hz, and the typical deviation depends on the empirical formula used in the calculation. In the case of chitin molecules, the starting position of N-acetyl group does not correspond to the most favorable position. Therefore, during the first 12 ns of equilibration, the monotonic changes of the torsion angle χ_2 from ~ − 10° to ~ − 53°occurred, which resulted in the broad range of the $^3J_{H2,H21}$ values. After equilibration (during the period of 12–19 ns), the perfect agreement between the calculated $^3J_{H2,H21}$ value of 9.05 Hz with the experimental value of 9.07 Hz takes place.

The good agreement between the torsion angles for the crystal structures and the XRD data, between the $^3J_{HH}$ constants for polymer molecules in an aqueous media and the NMR data, as well as the agreement between angle values and rotamers energy distribution with the experimentally verified results of previous MD study allows us to conclude that the force field parameters proposed here provide the proper description of the conformational properties of chitosan, chitin, and their derivatives.

Conformational transitions of glucopyranose rings

It is well known that the conformations of glucopyranose rings are very sensitive to the intramolecular force field parameters [17, 20, 21]. Although we did not change these parameters during our modification of 56A$_{CARBO}$, the changes in the

Table 9 Lennard-Jones interaction parameters

Atom type	$[C_6]^{1/2}$ (kJ mol^{-1} nm^6)$^{1/2}$	$[C_{12}]^{1/2}$ (nonpolar) (kJ mol^{-1} nm^6)$^{1/2}$	$[C_{12}]^{1/2}$ (polar) (kJ mol^{-1} nm^6)$^{1/2}$	$[C_{12}]^{1/2}$ (neighbor) (kJ mol^{-1} nm^6)$^{1/2}$	$[C_{12}]^{1/2}$ (neighbor) (kJ mol^{-1} nm^6)$^{1/2}$
N	$4.936 \cdot 10^{-2}$	$1.523 \cdot 10^{-3}$	$1.943 \cdot 10^{-3}$	$4.936 \cdot 10^{-2}$	$1.301 \cdot 10^{-3}$
NT	$4.936 \cdot 10^{-2}$	$1.523 \cdot 10^{-3}$	$2.250 \cdot 10^{-3}$	$4.936 \cdot 10^{-2}$	$1.301 \cdot 10^{-3}$

Table 10 Parameters for special intramolecular Lennard-Jones interactions

Pattern	C_6 (kJ mol^{-1} nm^6)	C_{12} (kJ mol^{-1} nm^6)	Interaction
H-N-Xr-Xr-Xr	0.0	$0.35 \cdot 10^{-6}$	H21-O5, H22-O5, H23-O5
H-NT-Xr-Xr-Xr			H21-C4, H22-C4, H23-C4
N-Xr-Xr-CHr	$3.392513 \cdot 10^{-3}$	$2.5 \cdot 10^{-6}$	N2-C4
NT-Xr-Xr-CHr			

charge groups and atom types can influence the conformational properties implicitly. The most sensitive property of β-D-glucopyranose is the conformational transition $^4C_1 \rightarrow {}^1C_4$. Like glucose, the most favorable conformation of chitosan and chitin is $^4C_1$. The conformation of six-membered rings is described with three Cremer-Pople (CP) parameters [50]: meridian angle φ, azimuthal angle θ, and radius Q. Transition $^4C_1 \rightarrow {}^1C_4$ corresponds to the changes in θ from 0° to 180° (ideal values for $^4C_1$ and $^1C_4$, respectively). In order to evaluate the energy of such a transition with the new $56A_{CARBO\_CHT}$ parameters, we carried out the PES profile exploration along the coordinate θ using the metadynamics calculations. The Gaussian umbrella potentials were applied to the chitosan tetramers in the 3D periodic rectangular box (5.1 × 3.8 × 3.4 nm) providing the movement along the reaction coordinate. The calculations have been performed using GROMACS with PLUMED plugin (height of Gaussian hills is 60 kJ mol^{-1}, bias factor is 5.0, temperature is 300 K), the length of MD trajectory was 10 ns, equilibration 500 ps, step 1 fs, temperature was 300 K.

The calculated PES profiles for the $^4C_1 \rightarrow {}^1C_4$ transitions in the five types of modified rings are shown in Fig. 7. As seen from the figure, for all the modified residues, the most

Table 11 Characterization of rotation of exocyclic groups

Angle	$56A_{CARBO\_CHT}$ chitosan whole crystal	$56A_{CARBO\_CHT}$ chitosan crystal (internal chain only)	$56A_{CARBO\_CHT}$ chitosan molecule	$56A_{CARBO\_CHT}$ chitin molecule	Literature		
					value	method	ref.
Average angle values							
ω	151.4	167.8	113.1	117.4	176.0	crystal XRD	[35]
					−170.9	crystal XRD	[33]
χ_6	174.4	154.7	156.3	155.9	–	–	–
χ_2[a]	–	–	–	−170.8 −168,4[d]	180 ± 21	solution MD	[45]
Rotamers distribution *g*+: *t*: *g*-, %							
ω	30: 66: 4	17: 81: 2	60: 37: 3	56: 42: 2	53: 45: 2	solution MD	[45]
					37: 60: 3[c]	solution MD	[12]
					35: 60: 4[c]	solution MD	[17]
χ_6	21: 65: 14	50: 31: 19	35: 50: 15	32: 54: 13	32: 45: 23	solution MD	[45]
					22: 25: 53[c]	solution MD	[12]
					22: 26: 52[c]	solution MD	[17]
χ_2[a]	–	–	–	27: 40: 33 14: 67: 19[d]	0: 87: 13	solution MD	[45]
$^3J_{HH}$ coupling constants, Hz							
$^3J_{H5,H6R}/{}^3J_{H5,H6S}$[b] (Stenutz eq.)	6.93 / 2.45	7.84 / 2.14	4.49 / 2.24	4.75 / 2.16	5.57 / 1.85	NMR study	[47]
					5.95 / 2.27[c]	NMR study	[48]
$^3J_{H5,H6R}/{}^3J_{H5,H6S}$[b] (Tafazzoli eq.)	7.15 / 2.53	8.06 / 2.24	4.87 / 2.33	5.13 / 2.26	6.0 / 2.1[c]	NMR study	[49]
$^3J_{H2,H21}$[a]	–	–	–	7.45 9.05[d]	9.07 10.39	NMR study calc from MD	[45]

ω is C4–C5–C6–O6, ώ is O5-C5-C6-O6, χ_6 is C5–C6–O6–HO6, χ_2 is H21–N2–C2–H_{C2}

[a] atom H2 is implicit in the force filed and it was derived from coordinate of atoms C3, C2, C1 via Z-matrix parameters obtained from quantum chemistry for b-D-N-acetyl-glucoseamine

[b] atoms H6S and H6R are implicit in force field, values of $^3J_{HH}$ was calculated using the equations of Stenutz and Tafazzoli via angle ώ. The distribution of angle ώ is 67:4:30, 82:2:16, 40:3:57, and 43:2:55 for chitosan crystal, internal chain in crystal, free molecules of chitosan and chitin, respectfully

[c] values are for b-D-glucopyranose or its derivatives, not for chitosan or chitin

[d] data is only for trajectory 12–19 ns of modeling

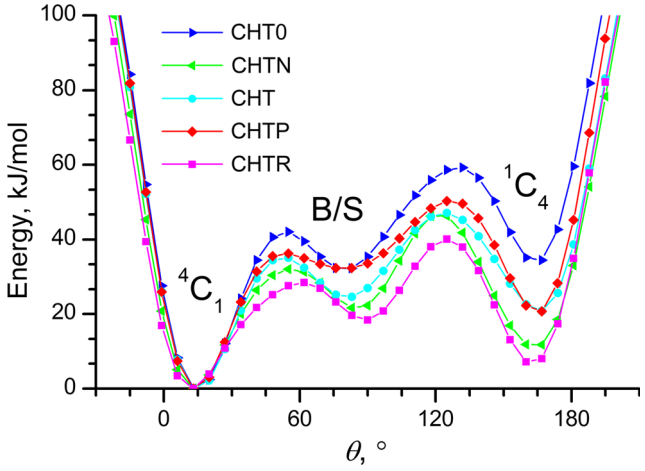

Fig. 7 PES profile along the Cremer-Pople θ parameter for developed chitosan residues

favorable conformation is $^4C_1$, in agreement with experimental data. The $^1C_4$ conformation is higher in energy by 10–30 kJ mol^{-1} depending on the ring type, the calculated activation barrier for the $^4C_1$ ➔ $^1C_4$ transition is in the range of 40–60 kJ mol^{-1}. The mean value and standard deviation of θ inside the crystal is 9.5° ± 5.2°, for the free molecules in a solution is 10.7° ± 6.0°. These values are in good agreement with the results of the initial force field 56A$_{CARBO}$, as well as with the experimental study of Sattelle and Almond [51]. We conclude that the modification of the charges and charge groups do not influence the conformation properties of glucopyranose rings.

Structural parameters of glycosidic bonds

Another important structural characteristic of the biopolymers is the structural motifs formed in the polymeric chains due to the statistical distributions of torsion angles of the glycosidic bond: O5-C1-O1-C4' (φ) and C1-O1-C4'-C3' (ψ). Some authors [52] use torsion angle C1-O1-C4'-C5' (ψ') instead of C1-O1-C4'-C3' (ψ). The experimental values of these angles in crystalline packings are determined from the XRD data [33, 35, 52, 53]. Additionally, the MD estimates of glycosidic bond parameters in the aqueous solution were reported by Franca et al. [18, 19]. In order to evaluate the new force field parameters, we calculated the distributions of the glycosidic bond parameters φ, ψ, and ψ' for the chitosan nanocrystals placed into the water media and for the chitosan and chitin polymers in aqueous solutions.

The results of MD calculations are given in Table 12 in comparison with the available experimental data and the results of previous MD calculations. In the case of nanocrystal calculations, the deviation from the average XRD values is about 15% of the measured angle. As seen from Fig. 8a, this deviation is completely within the region of statistically scattered angle values. It should also be noted that this rather remarkable disagreement of 15% can partially be a consequence of the real physical effect—a twist-like distortion of nanocrystals in the aqueous solution. This twist-like distortion of nanocrystals always arises after its equilibration inside the water environment and was also reported by other authors during the simulations of cellulose nanocrystals in water [54]. For the free polymeric molecules in a solution the average values of φ and ψ are distinguished from the crystal XRD data more significantly, due to the higher flexibility of solvated molecules in comparison with the crystalline packing. The calculated angle distribution (Fig. 8b and c) coincide well with the data of Franca et al. [18, 19] obtained for the chitosan polymers. Both for chitin and chitosan molecules in a solution, we observed additional population in the region of φ = ~50°, ψ = ~ − 50°. This fact is in good agreement with the calculated free energy maps reported by Plazinski et al. [17] where the additional unfavorable local minimum takes place in the region of these values for cellobiose. As a whole, the agreement with the available experimental data and the calculation results reported earlier allows us to make a conclusion on the proper

Table 12 Characterization of glycosidic linkage conformation angles

Angle	56A$_{CARBO_CHT}$ Chitosan crystal	56A$_{CARBO_CHT}$ Chitosan molecule	56A$_{CARBO_CHT}$ Chitin molecule	Experimental values (XRD)
φ	−83.4	−69.5	−70.7	−96.3 [35]
				−92.1 [33]
				−92.0 [52]
				−98.3 [53]
ψ	102.5	110.5	110.5	92.0 [35]
				94.0 [33]
				96.2 [53]
ψ'	−140.0	−127.1	−129.5	−146.6 [35]
				−147.0 [33]
				−148.0 [52]
				−143.0 [53]

φ is O5–C1–O1–C4', ψ is C1–O1–C4'–C3', ψ' is C1–O1–C4'– C5'

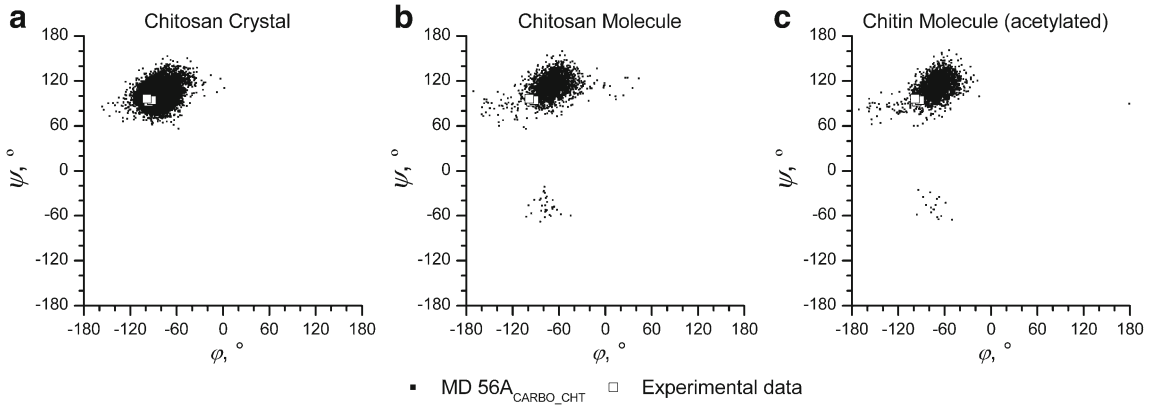

Fig. 8 The distribution of torsion angles φ and ψ for the chitosan crystal in water (**a**), chitosan single molecule in water (**b**) and chitin (acetylated) single molecule in water (**c**)

description of glycosidic bond properties with the modified force field parameters.

Thus, in comparison with the force fields used earlier for the MD simulations of chitosan polymers (e.g., MMX force field used in [45] that never was specially parametrized for carbohydrate polymers), the modified 56A$_{CARBO_CHT}$ force field parameters provides a good description of properties of β-D-glucosamine polymer chains, is applicable for numerous types of biological systems including proteins, and compatible with free distributed high performance software like GROMACS.

Modeling of the solution of chitosan crystal

Testing of modified force field based on comparison with thermodynamic dissolution functions is complicated by the fact that experimental values were obtained for non-crystalline (glass-like) states of biopolymers with uncontrolled degree of initial hydration and protonation which have significant effects on dissolution heat values. Thus, direct comparison of experimental and calculated thermodynamic parameters turns out to be impossible. Therefore, verification of the obtained force field parameters in this work was based not on comparison of dissolution heat values but on analysis of dissolution kinetics at different initial conditions of the polymer and conformational behavior of polymer chains in the solution.

Chitosan is soluble in acid environments at pH < 6.7 which is explained by protonation of amino groups in acid environment. Coulomb repulsion forces emerge between protonated amino groups of different chains; these forces increase proportionally with the number of protonated groups. When these forces exceed intermolecular attraction forces holding the

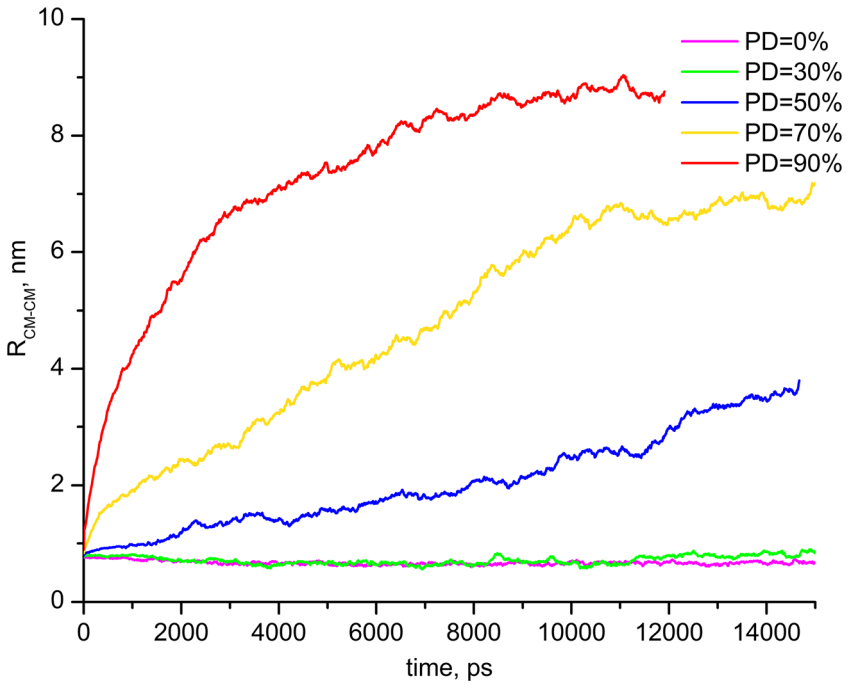

Fig. 9 The average distance between the mass centers (R_{CM-CM}) of polymer chains vs. time for different protonation degrees

chains together, the chitosan structure breaks down. Thus, the pH value when dissolution begins is a measure of subtle balance between the interchain attraction due to hydrogen bonds and dispersion interaction and the Coulomb repulsion of the charged groups.

Molecular dynamics simulation of chitosan crystal model dissolution with different degree of protonation in water was performed on the chitosan model nanocrystals using the modified force field (original T3 dihedral parameters were used in the test calculations presented here). The calculations were conducted at five different degrees of protonation: 0, 30, 50, 70 and 90%. Positions of protonated groups in the chitosan chains were chosen randomly (in the case of 90% protonation degree all groups were protonated except the terminal ones).

The results of the molecular dynamics simulation show that the presence of fully deprotonated nanocrystal corresponding to chitosan staying in the alkaline medium was featured only by the low torsional deformation of the initial crystal without its dissociation into separate chains. The nanocrystal deformation corresponded completely to the cellulose crystals twisting which was previously discovered in the molecular dynamics study [54].

In the case of unprotonated chitosan crystals and at the protonation degree (PD) of 30%, only strong deformation and loosening of crystal structure without dissociation were observed. This means that the Coulomb repulsion energy between positively charged chains is not strong enough to destroy the system of hydrogen bonds in crystal.

At the protonation degree of 50%, the crystal dissociation occurs during about 15 ns resulting in the formation of an unordered bunch of chitosan chains. In this bunch, the chains were held together with the non-protonated amino group regions. Extremely fast crystal dissolution occurs with PD = 70 and PD = 90%. In the case of 90% protonation, the quick dissociation of the crystalline structure took place during 3–5 ns of simulation, and the formation of a highly homogenized mixture of chitosan chains occurred in 8 ns.

In all cases of dissociation, the chitosan chains held their distorted linear shape without turning into globules. This fact is in agreement with the data of ref. [5] stating that the formation of globules takes place on relatively long and low-protonated polymer sections while the protonated regions remain linear.

Two indicators were selected for quantitative characterization of dissolution degree—the average distance between the mass centers of separate chains $R_{CM\text{-}CM}$ and the average distance between the separate units of different chains $R_{L\text{-}L}$. These indicators behave in a similar fashion. The variation of $R_{CM\text{-}CM}$ in time is shown in Fig. 9.

As evident from Fig. 9, the nanocrystal dissociation begins between 30 and 50% protonation of chitosan chains which corresponds to the pH value of ~6.8 and 6.4 respectively. This result is in good agreement with the experimental value pH = 6.2–6.7 when the dissolution of chitosan with molecular weight of 60–1370 kDa starts. [55–57] The good agreement between the calculated and experimental data confirms that the thermodynamic parameters of chitosan chain-chain and chain-solvent interaction, in the aqueous solution of different acidity, have been described correctly.

This conclusion is also supported by the results of a more detailed study of the chitosan dissolution process performed for more realistic systems under variation of chain lengths, temperatures, starting structures, and simulation times. Details of this study will be reported in a separate publication.

Conclusions

The $56A_{CARBO}$ force field has been extended to polyaminoglycans by adding the force field parameters of the residues corresponding to aminopyranose, its N-protonated form, its N-acetylated derivatives, and polymer chain terminators. Force field parameters have been adjusted on the basis of quantum chemical calculations of charge distribution of model systems. The test calculations performed for the model chitosan crystals in water with different chain protonation degrees demonstrate a good agreement with the available data on kinetics of chitosan dissolution in aqueous solutions of different acidity. The modified force field allows performing the molecular dynamic calculations of chitosan polymers with different protonation degrees and can also be applied to other N-substituted derivatives of chitosan using the corresponding force field parameters of the substituting groups. The test calculations of the conformational properties of chitosan chains in the form of nanocrystals or the polymers in aqueous media are in good agreement with the available experimental or calculated data. The modeling of the chitosan crystal dissolution process performed with the new force field parameters represent the experimentally measured pH value providing chitosan solubility. The extended force field ($56A_{CARBO\_CHT}$) files can be downloaded from the web-site of the Theoretical Chemistry Group of N.I. Lobachevsky State University of Nizhny Novgorod (http://www.qchem.unn.ru/md-simulations-and-force-field-development/).

Acknowledgements This work was partially supported by the Russian Foundation for Basic Research (Project No. 14-03-00585). The authors acknowledge the computer facility of the University of Nizhny Novgorod for providing the resources on the "Lobachevsky" supercomputer. We also express our gratitude to one of the anonymous reviewers for his/her attention, time, and valuable suggestions on the improvement of the manuscript.

References

1. Aydın RST, Pulat M (2012) 5-fluorouracil encapsulated chitosan nanoparticles for pH-stimulated drug delivery: evaluation of controlled release kinetics. J Nanomater 2012:10
2. Patel MP, Patel RR, Patel JK (2010) Chitosan mediated targeted drug delivery system: a review. J Pharm Pharm Sci 13(4):536–557

3. Riva R, Ragelle H, Rieux A et al. (2011) Chitosan and chitosan derivatives in drug delivery and tissue engineering. In: Jayakumar R, Prabaharan M, Muzzarelli RAA (eds) Chitosan for biomaterials II. Springer, Berlin, pp. 19–44
4. Ghaz-Jahanian M et al. (2015) Application of chitosan-based Nanocarriers in tumor-targeted drug delivery. Mol Biotechnol 57(3):201–218
5. Pedroni VI et al. (2003) Chitosan structure in aqueous solution. Colloid Polym Sci 282(1):100–102
6. Pedroni VI, Gschaider ME, Schulz PC (2003) UV spectrophotometry: improvements in the study of the degree of acetylation of chitosan. Macromol Biosci 3(10):531–534
7. Li Q-X et al. (2006) Electrolytic conductivity behaviors and solution conformations of chitosan in different acid solutions. Carbohydr Polym 63(2):272–282
8. Noid WG (2013) Perspective: coarse-grained models for biomolecular systems. J Chem Phys 139(9):090901
9. Pigaleva MA et al. (2014) Stabilization of chitosan aggregates at the nanoscale in solutions in carbonic acid Macromolecules 47(16): 5749–5758
10. Glukhova OE, et al (2015) Structure and properties of composites based chitosan and carbon nanostructures: atomistic and coarse-grained simulation
11. Kossovich E et al. (2014) Hybrid coarse-grained/atomistic model of "chitosan + carbon nanostructures" composites. J Mol Model 20(10):1–7
12. Hansen HS, Hunenberger PH (2011) A reoptimized GROMOS force field for hexopyranose-based carbohydrates accounting for the relative free energies of ring conformers, anomers, epimers, hydroxymethyl rotamers, and glycosidic linkage conformers. J Comput Chem 32(6):998–1032
13. Lins RD, Hunenberger PH (2005) A new GROMOS force field for hexopyranose-based carbohydrates. J Comput Chem 26(13):1400–1412
14. Oostenbrink C et al. (2004) A biomolecular force field based on the free enthalpy of hydration and solvation: the GROMOS force-field parameter sets 53A5 and 53A6. J Comput Chem 25(13):1656–1676
15. Foley BL, Tessier MB, Woods RJ (2012) Carbohydrate force fields. Comput Mol Sci 2(4):652–697
16. Schmid N et al. (2011) Definition and testing of the GROMOS force-field versions 54A7 and 54B7. Eur Biophys J Biophys Lett 40(7):843–856
17. Plazinski W, Lonardi A, Hünenberger PH (2016) Revision of the GROMOS 56A6CARBO force field: improving the description of ring-conformational equilibria in hexopyranose-based carbohydrates chains. J Comput Chem 37(3):354–365
18. Franca EF et al. (2008) Characterization of chitin and chitosan molecular structure in aqueous solution. J Chem Theory Comput 4(12):2141–2149
19. Franca EF, Freitas LCG, Lins RD (2011) Chitosan molecular structure as a function of N-acetylation. Biopolymers 95(7):448–460
20. Plazinski W, Drach M (2014) The dynamics of the conformational changes in the hexopyranose ring: a transition path sampling approach. RSC Adv 4(48):25028–25039
21. Plazinski W, Drach M (2015) The influence of the hexopyranose ring geometry on the conformation of glycosidic linkages investigated using molecular dynamics simulations. Carbohydr Res 415:17–27
22. Malde AK et al. (2011) An automated force field topology builder (ATB) and repository: version 1.0 J Chem Theory Comput 7(12): 4026–4037
23. Gasteiger J, Marsili M (1980) Iterative partial equalization of orbital electronegativity—a rapid access to atomic charges. Tetrahedron 36(22):3219–3228
24. Mayo SL, Olafson BD, Goddard WA (1990) DREIDING: a generic force field for molecular simulations. J Phys Chem 94(26):8897–8909
25. Singh UC, Kollman PA (1984) An approach to computing electrostatic charges for molecules. J Comput Chem 5(2):129–145
26. Breneman CM, Wiberg KB (1990) Determining atom-centered monopoles from molecular electrostatic potentials. The need for high sampling density in formamide conformational analysis. J Comput Chem 11(3):361–373
27. Angyal SJ (1968) Conformational analysis in carbohydrate chemistry. I. Conformational free energies. The conformations and α : β ratios of aldopyranoses in aqueous solution. Aust J Chem 21(11):2737–2746
28. Angyal SJ (1969) The composition and conformation of sugars in solution. Angew Chem Int Ed Engl 8(3):157–166
29. Angyal SJ (1984) The composition of reducing sugars in solution. Adv Carbohydr Chem Biochem 42:15–68
30. Vijayalakshmi KS, Rao VSR (1972) Theoretical studies on the conformation of aldopyranoses. Carbohydr Res 22(2):413–424
31. 56A_CARBO4GROMACS. Available from: http://www.gromacs.org/@api/deki/files/200/=56a_CARBO4GROMACS.rar
32. MD Simulations and Force Field development. Available from: http://www.qchem.unn.ru/md-simulations-and-force-field-development/
33. Okuyama K et al. (1997) Molecular and crystal structure of hydrated chitosan. Macromolecules 30(19):5849–5855
34. Ogawa K, Yui T, Okuyama K (2004) Three D structures of chitosan. Int J Biol Macromol 34(1–2):1–8
35. Yui T et al. (1994) Molecular and crystal structure of the anhydrous form of chitosan. Macromolecules 27(26):7601–7605
36. Páll S, et al (2015) Tackling exascale software challenges in molecular dynamics simulations with GROMACS. In: Markidis S and Laure E (ed) Solving software challenges for Exascale: International Conference on exascale applications and software, EASC 2014, Stockholm, Sweden, April 2–3, 2014, Revised Selected Papers. Springer , Cham, p 3–27
37. Bonomi M et al. (2009) PLUMED: a portable plugin for free-energy calculations with molecular dynamics. Comput Phys Commun 180(10):1961–1972
38. Berendsen HJC (1991) Transport properties computed by linear response through weak coupling to a bath. In: Meyer M, Pontikis V (eds) Computer simulation in materials science: interatomic potentials, simulation techniques and applications. Springer, Dordrecht, pp. 139–155
39. Darden T, York D, Pedersen L (1993) Particle mesh Ewald: an N·log(N) method for Ewald sums in large systems. J Chem Phys 98(12):10089–10092
40. Essmann U et al. (1995) A smooth particle mesh Ewald method. J Chem Phys 103(19):8577–8593
41. Hockney RW, Goel SP, Eastwood JW (1974) Quiet high-resolution computer models of a plasma. J Comput Phys 14(2):148–158
42. Hess B et al. (1997) LINCS: a linear constraint solver for molecular simulations. J Comput Chem 18(12):1463–1472
43. Stenutz R et al. (2002) Hydroxymethyl group conformation in saccharides: structural dependencies of 2JHH, 3JHH, and 1JCH spin−spin coupling constants. J Org Chem 67(3):949–958
44. Tafazzoli M, Ghiasi M (2007) New Karplus equations for 2JHH, 3JHH, 2JCH, 3JCH, 3JCOCH, 3JCSCH, and 3JCCCH in some aldohexopyranoside derivatives as determined using NMR spectroscopy and density functional theory calculations. Carbohydr Res 342(14):2086–2096
45. Mobli M, Almond A (2007) N-acetylated amino sugars: the dependence of NMR 3J(HNH2)-couplings on conformation, dynamics and solvent. Org Biomol Chem 5(14):2243–2251
46. Halgren TA (1996) Merck molecular force field. I. Basis, form, scope, parameterization, and performance of MMFF94. J Comput Chem 17(5–6):490–519
47. Roslund MU et al. (2008) Complete assignments of the (1)H and (13)C chemical shifts and J(H,H) coupling constants in NMR spectra

of D-glucopyranose and all D-glucopyranosyl-D-glucopyranosides. Carbohydr Res 343(1):101–112
48. Blundell CD et al. (2009) Investigating the molecular basis for the virulence of *Escherichia coli* K5 by nuclear magnetic resonance analysis of the capsule polysaccharide. J Mol Microbiol Biotechnol 17(2):71–82
49. Yoshihiro Nishida HO, Meguro H (1984) 1H-NMR studies of (6r)- and (6s)-deuterated D-hexoses: assignment of the preferred rotamers about C5C6 bond of D-glucose and D-galactose derivatives in solutions. Tetrahedron Lett 25(15):1575–1578
50. Cremer D, Pople JA (1975) General definition of ring puckering coordinates. J Am Chem Soc 97(6):1354–1358
51. Sattelle BM, Almond A (2011) Is N-acetyl-d-glucosamine a rigid 4C1 chair? Glycobiology 21(12):1651–1662
52. Yui T et al. (2007) Exhaustive crystal structure search and crystal modeling of beta-chitin. Int J Biol Macromol 40(4):336–344
53. Gardner KH, Blackwell J (1975) Refinement of the structure of β-chitin. Biopolymers 14(8):1581–1595
54. Paavilainen S, Rog T, Vattulainen I (2011) Analysis of twisting of cellulose nanofibrils in atomistic molecular dynamics simulations. J Phys Chem B 115(14):3747–3755
55. Alvarenga ESD (2011) Characterization and properties of chitosan, in biotechnology of biopolymers. In: Elnashar M (ed) InTech: Janeza Trdine 9. 51000 Rijeka, Croatia, pp. 91–108
56. Mao S et al. (2004) The depolymerization of chitosan: effects on physicochemical and biological properties. Int J Pharm 281(1–2): 45–54
57. Wang QZ et al. (2006) Protonation constants of chitosan with different molecular weight and degree of deacetylation. Carbohydr Polym 65(2):194–201